REALISTIC MULTIMEDIA: FROM PHYSICAL MODELS TO INSTRUCTIVE MULTIMEDIA CONTENT

Ioannis Pachoulakis

ABSTRACT
Multimedia technologies are invaluable in generating realistic content and applications which increase the effectiveness and communication impact of research results. The functional keyword "realistic" means content that is based on physical modeling and, therefore, is physically sound. The present article reports on a novel custom-built toolkit intended to train budding astronomers into simulating and visualizing the composite 3D structure of winds from hot close double stars by implementing a technique which is similar to multi-directional medical tomography. In such hot binaries, the light sources that scan and probe the composite wind volume are the bright "surfaces" (photospheres) of the individual stars. Then, as the Keplerian orbit is traced out and the geometry presented to the observer varies, each star constitutes an analyzer upon its companion's wind. In contrast to medical tomography, however, these targets are too far to be resolved spatially so we resort to modeling the ultraviolet (UV) spectral lines of certain wind ions (e.g., N^{+4}, Si^{+3}, C^{+3}) whose shapes vary with Keplerian phase as the stars revolve around their common centre of mass. The flagships of the toolkit are the Spectrum Analyzer and Animator (SA^2) and the Binary 3D Renderer (B3dR). The first tool, the SA^2, automates (a) the derivation of light curves from the observed spectra and (b) the generation of synthetic binary wind-line profiles which reproduce the morphologies and variabilities of the observed wind profiles. After the composite wind structure of a binary has been recovered, the B3dR is employed to visualize the results and simulate the revolution of the entire system (stars, winds and wind-interaction effects) around the common centre of mass. The B3dR thus repackages the end product of a lengthy physical modeling process to generate realistic multimedia content and enable the presentation of the 3D system from the point of view of an observer on Earth as well as from any other observer location in the Galaxy.

KEYWORDS
Realistic Multimedia Content, Physical Models, 3D visualization.

INTRODUCTION

Contrary to the casual observer's impression of a night sky full of single stars, most stars are in fact composed of two stars which revolve around their common centre of mass. In spectroscopic binaries the stars are so close to each other that they remain unresolved even through a telescope: their binary nature is recovered only from their spectra thanks to the Doppler Effect. Of these spectroscopic binaries, the subset of eclipsing binaries is of the greatest importance, as their study discloses accurate masses and radii, which provide the prime test bed of stellar models. Hot, massive (O and B) Main Sequence stars are at least 10 times more massive and much hotter ($T \geq 30{,}000$ K) than the sun, so that material from their surface is blown away by radiation pressure, forming stellar winds composed of charged particles (protons, electrons and ions) accelerated to supersonic speeds. A scaled-down version of the phenomenon is our own solar wind, whose occasional violent eruptions give rise to gusts which reach Earth, are deflected by its geomagnetic field and cause magnetic storms, magnificent auroras and interruptions in telecommunications.

It is interesting to note that continuum photons from the stellar photosphere travel through a wind shell virtually unimpeded, i.e., scattering of continuum photons by wind material is negligible. This means

that if one were to observe such hot binaries from a sufficiently short distance through spectral "glasses" which allow line-blanketed continuum to pass but which exclude wind-line photons, then the individual photospheric disks would be resolved and no surrounding wind shell would be discerned. On the other hand, through "glasses" which isolate wind activity, the photospheric disks would seem embedded in wind material and would be partially or even totally obscured. Accordingly, the components of a binary may appear larger than the photospheric disks, depending on the spectral bandpass of observation.

In addition, as the Keplerian orbit is traced out, the geometry presented to the observer varies and each star constitutes an analyzer upon its companion's wind, probing that wind's structure in a process reminiscent of tomography. Indeed, stellar wind studies use Doppler-resolved spectral signatures to reconstruct the composite wind from a sequence of spectra recorded as the component stars coast along their orbits. The modeling process detailed in this article uses the spectral signatures of prominent wind ions such as those of N^{+4}, Si^{+3}, C^{+3} which trace the wind structure forming the well-known wind lines of NV, SiIV and CIV respectively, and whose profiles generally vary as the stars revolve and as wind inhomogeneities form, propagate and evolve.

Using UV spectra secured by the International Ultraviolet Explorer (IUE) satellite at various orbital phases, this article shows how to model these spectral lines, reconstruct the 3D composite wind structure and simulate the motion of the system around a common center of mass. The output is realistic content that can be incorporated in multimedia applications (e.g., Flash presentations) and aims at increasing the effectiveness and communication impact of research results. The article is organized in the following way. The next section introduces the spectroscopic binary HD159176 which is used as a showcase of the methodology and presents pertinent observational material. The remaining sections show how to model and visualize the 3D winds and additional density enhancements followed by a discussion of the results obtained.

THE TARGET AND THE OBSERVATIONAL MATERIAL

The showcase of our analysis is HD159176, which is the brightest object (V = + 5.68, B-V = +0.04) in the Milky Way open cluster NGC 6383 (Lloyd-Evans, 1978), and is classified as O7V + O7V by Hiltner, Garrison and Schild (1969) and as O6V + O6V by Levato (1975). The observational material includes V-band photometry from ground plus 38 well-exposed high-resolution spectral images recorded by the Short Wavelength Primary (SWP) camera of the International Ultraviolet Explorer (IUE) satellite. Of these, the first 8 were secured in 1979 and 1980 through the small aperture and the remaining 30 during a 1992 observing run through the large-aperture with dense coverage around quadrature phases. A sample spectrum very near quadrature phase appears in Figure 1.

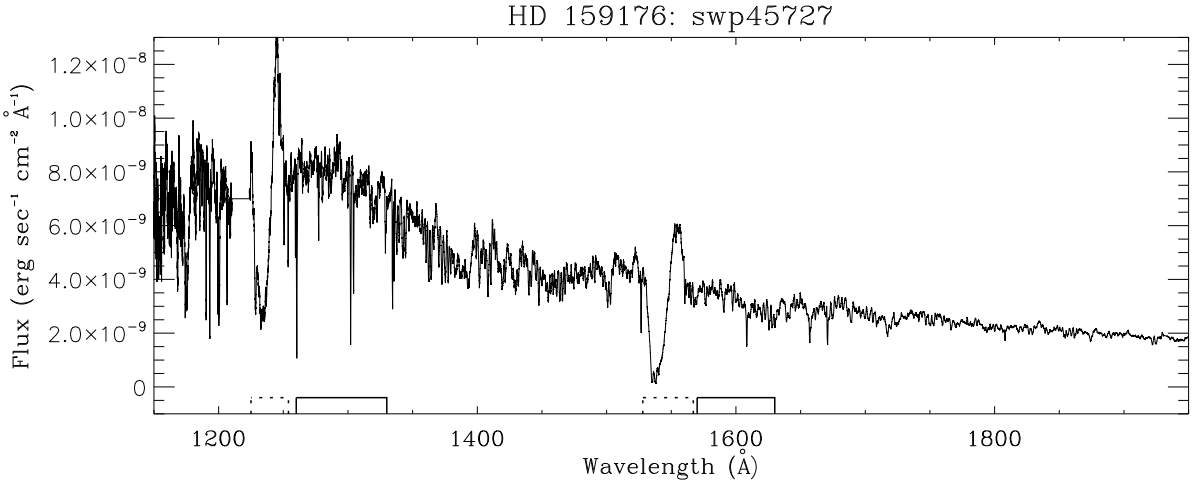

Figure 1. Spectrum showing continuum and wind-affected bandpasses (continuous and dashed lines).

The 30 more recent images were secured in the course of a single observing run and in rapid succession, thus providing an almost real-time account of the binary's spectral changes in phase and in time. The spectral sensitivity of the SWP camera is variable between 1150Å and 1950Å, and the S/N ratio for these well-exposed SWP images is ≈ 15. As an initial step of the analysis, all images were de-reddened with the aid of standard Data Analysis Center (IUEDAC) routines using the Savage & Mathis (1979) galactic extinction curve and a color excess E(B-V) = +0.36.

Table 1. Orbital and photospheric elements of the component stars of HD159176.

Parameter	**Value**	**Parameter**	**Value**
Spectral Class	O6V + O7V	$\imath$	50^o
Period	3.366764 days	$R_{1,2}$ (Ro)	9.8 , 9.3
e	0.0	$v\sin i$ (km/sec)	150, 150
ω (degrees)	Undefined	g_c / g_{grav}	0.06 , 0.06
M_2 / M_1	0.99	v_{rot} / v_{esc}	0.18 , 0.17
$\alpha\sin i$ (R_o)	9.8 , 9.3	$F_{1,2}$	1.3 , 1.4

A very precise radial velocity curve of this young binary has been discussed by Stickland, Koch, Pachoulakis and Pfeiffer (1993) who derive the orbital elements listed in Table 1: eccentricity (e), periastron (ω), mass ratio (M_2/M_1) and $\alpha\sin i$, and a systemic velocity of about +10 km/s, compatible with the kinematics of other members of NGC 6383. The published projected rotational speed ($v\sin i$) is also listed (line 3, right pane), from which the ratio of centrifugal to gravitational acceleration (g_c/g_{grav}) for each stellar component follows readily, as well as the ratios of rotational to escape velocities (v_{rot}/v_{esc}) and the revolution to spin periods (F_1 and F_2).

In addition, Pachoulakis (1996) presents combined photometric and radial velocity solutions yielding orbital elements identical (within errors) to those of Stickland, Koch, Pachoulakis and Pfeiffer (1993) and argues for a nominal inclination of 50^o. With individual stellar radii of about 0.25*a*, where *a* is the semi-major axis of the Keplerian orbit, the stars are sufficiently large and close enough for an ellipsoidal variability pattern with an amplitude of 0.05m in the V band to be reported by Thomas (1975). That photometry spans 5 consecutive cycles of the binary and appears in Thomas and Pachoulakis (1994), supplemented with three UV light curves which display ellipsoidal variability with an amplitude of about 0.07m.

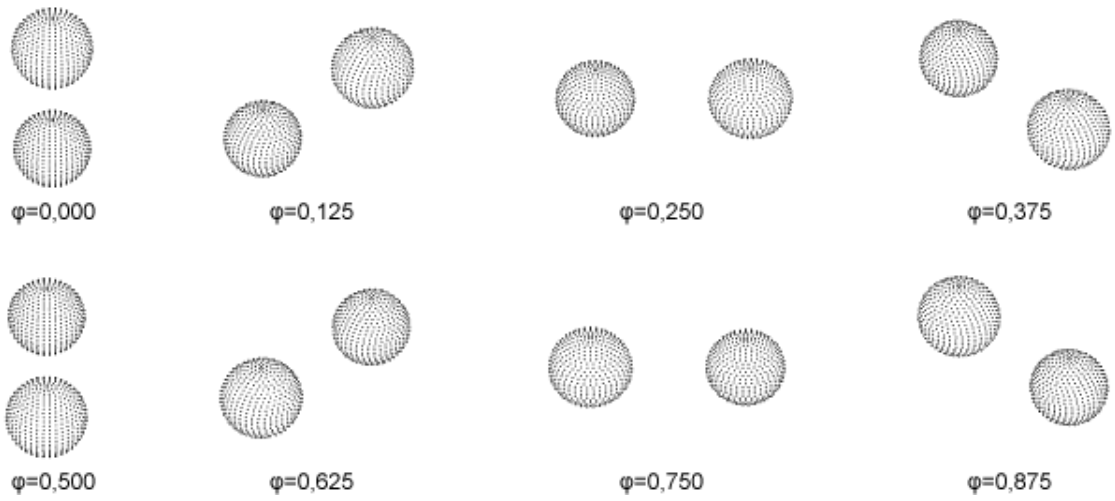

Figure 2. Snapshots showing the revolving 3D photospheres during the progress of one orbital cycle as seen from Earth, in steps of Δφ=0.125, starting at φ=0 at the top left.

Figure 2 shows a sequence of snapshots from a simulation showing how an observer sufficiently close to the target and along the line of sight from Earth would see the binary at continuum wavelengths. The reader may note that at continuum bandpasses the winds and clouds which surround the stars are invisible, so that the observer really sees just the two photospheres.

SYNTHETIC BINARY WIND-LINE PROFILES

The SEI (Sobolev with Exact Integration) method for calculating line profiles of spherically symmetric winds from single stars is described in Lamers, Cerruti-Sola and Perinoto (1987), hereafter LCP, and has been applied to O star winds (e.g., Groenewegen and Lamers, 1989, Groenewegen, Lamers and Pauldrach 1989) and to outflows from planetary nebulae (e.g., Perinotto, Cerutti-Sola and Lamers, 1989). The method allows for radiative interaction between the blue and red members of a doublet such as NV, SiIV and CIV and was applied in this article to generate synthetic binary wind-line model profiles as follows.

For a two-level atom/ion, the source function in SEI is written as

$$S_\nu = \frac{\delta_c(r)\cdot I_\nu^* + \varepsilon \cdot B_\nu(r)}{\delta + \varepsilon},$$

where I_ν^* is the intensity at frequency ν of the radiation leaving the stellar photosphere, B_ν is the Plank function in the wind, δ is the escape probability for line photons, δ_c is the penetration probability for continuum photons, and ε is the ratio of collisional to radiative de-excitations. The collisional term ε for the source function is negligible for resonance lines in O and B stars and is set to zero, accordingly. The relevant parameters employed by SEI to generate a model profile appropriate for a stellar wind from an O or B star are discussed directly below.

For a single star, the wind speed for a given ion is modeled by a β-type law:

$$w(r) = w_0 + (1 - w_0)\cdot(1 - 1/r)^\beta,$$

where $w(r)$ is the wind speed $v(r)$ normalized to v_∞, i.e., $w(r) = v(r) / v_\infty$, and w_0 is the normalized wind speed at the wind base. The parameter $w_{Gauss} \equiv v_{Gauss} / v_\infty$ mimics the occurrence of small-scale perturbations of the velocity law by introducing, at distance r, a Gaussian distribution of speeds centered on $w(r)$ with a half-width w_{Gauss}. A_{photB} and A_{photR} are the photospheric depths (in normalized flux) of the blue and red components of the doublet, respectively. Similarly, W_{photB} and W_{photR} are the photospheric widths of the blue and red members of the doublet. Because SEI does not solve the statistical equilibrium equations in the wind, an optical depth law is specified which has the following form (Equation 40 in LCP):

$$\frac{d\tau}{dw} = \frac{T_{Tot}}{I}\left(\frac{w}{w_1}\right)^{\alpha_1}\left[1 - \left(\frac{w}{w_1}\right)^{1/\beta}\right]^{\alpha_2}$$

The optical depth law so specified is quite versatile, with $\alpha_{1,2}$ acting as shaping parameters for the functional dependence of $d\tau/dw$ on wind speed w and, via the velocity law, for the dependence of $d\tau/dr$ on distance r. Furthermore, as observable line formation does not necessarily extend to v_∞, a parameter w_1 is introduced, which defines the extent of the wind in velocity space, in the sense that line formation ceases beyond $w = w_1$. T_{photB} and T_{photR} are the integrated radial optical depths for the blue and red components of the doublet, respectively. Finally, the integral

$$I = \int_{w_0/w_1}^{1} y^{\alpha_1}(1 - y^{1/\beta})^{\alpha_2}\,dy$$

is introduced for normalization, so that

$$\int_{w_0}^{w_1} \frac{d\tau}{dw} dw = T_{Tot}.$$

Figure 3 displays the build-up of wind speed (left panel) and the drop-off of optical depth (right panel) from the surface of a single star with the characteristics of the primary star of HD159176 using parameter values from Pachoulakis (1996).

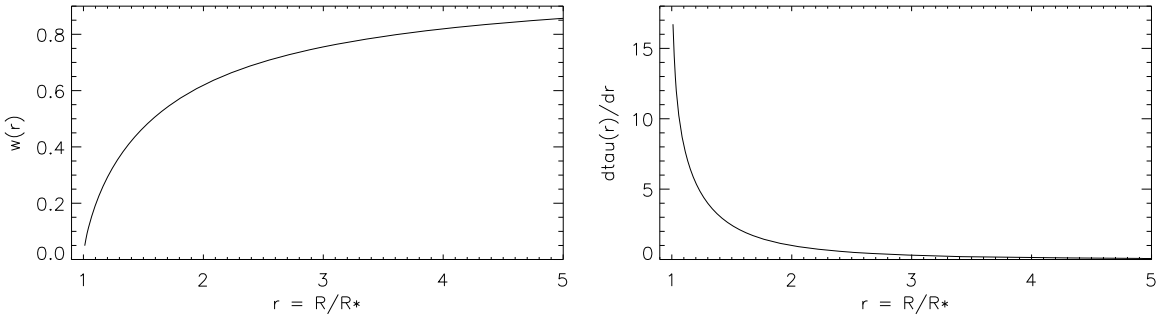

Figure 3. The build-up of wind speed (left panel) and the drop-off of optical depth (right panel).

In SEI, S_v is solved in the Sobolev approximation but the equation of transfer is integrated exactly along lines of sight with impact parameters $p \geq 0$ using equations (28) and (29) in LCP. The left panel of Figure 4 shows a schematic of an extended wind around a single star and the right panel shows the SEI single-star CIV wind-line profile (continuous curve). For any line of sight to a distant observer, the impact parameter p is the normalized distance from the star center. Then, as seen from Earth, the SEI model profile is the sum of:

- The pure emission contribution (dashed line in right panel) from the part of the wind with $p \geq 1$ (horizontally hatched projected area in left panel), plus
- The pure absorption contribution (dotted line in right panel) from the part of the wind directly in front of the star with $p < 1$ (cross-hatched projected area in left panel) as material accelerates in the direction to the observer. (The reader may note that the contribution to line formation of the part of the wind with $p < 1$ which is behind the star is zero as it is occulted by the stellar disk.)

For the extended, optically thick winds from early O-type stars like HD159176 both contributions to line formation (i.e., for $p \geq 1$ and for $p < 1$) are significant, the net result being the characteristic P-Cygni profile shown in the right panel of Figure 4 which combines absorption and emission. On the other hand, for late-O or early-B stars, most of the wind-line formation takes place within a shell of thickness just a small fraction of the stellar radius, so that the contribution to line formation for $p \geq 1$ dominates that for $p < 1$ and the net profile is an absorption feature.

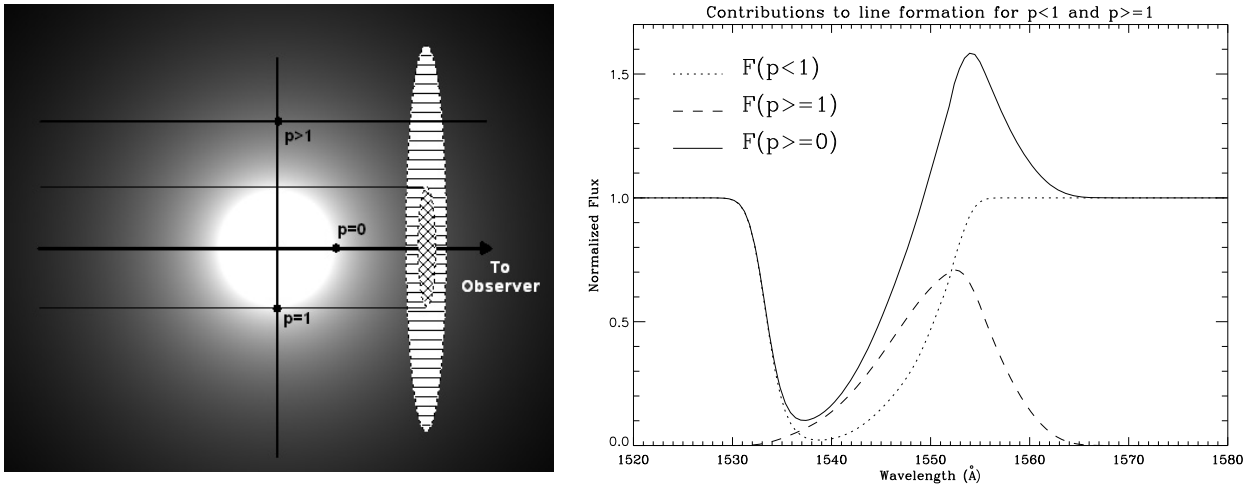

Figure 4. Schematic of an extended wind around a single star (left panel) and SEI wind-line profile (continuous curve in the right panel).

THE SPECTRUM ANALYZER AND ANIMATOR (SA^2)

The Spectrum Analyzer and Animator (SA^2), whose interface appears on Figure 5, automates the following procedure to generate a sequence of synthetic binary wind-line profiles to fit a sequence of observed wind-line profiles.

1. *Generation of single-star SEI profiles:* The stellar components of the binary are first "fitted" with individual single-star winds, which are assumed to be centered on their host stars. These steady-state, time-independent individual wind structures yield phase-independent single-star SEI profiles $F_{\{1\}}(\lambda)$ and $F_{\{2\}}(\lambda)$ for the primary and secondary star of the binary, respectively. Because a single-star SEI profile $F(\lambda)$ is the sum of the contributions for impact parameters impinging the photosphere ($p < 1$) and impact parameters not-impinging the photosphere ($p \geq 1$), then for star j=1,2:
$$F_j(\lambda) \equiv F_j(\lambda; p \geq 0) = F_j(\lambda; p < 1) + F_j(\lambda; p \geq 1)$$
2. *Doppler-shift of SEI profiles*: For every IUE spectrum at orbital phase φ, this second step entails the Doppler-shift of the individual phase-independent SEI profiles using radial velocities $RV_1(\varphi)$ and $RV_2(\varphi)$ for the stellar components that follow from published radial velocity solutions. This process yields the individual phase-dependent profiles $F_{\{1,2\}}(\lambda;\varphi)$:
$$F_j(\lambda;\phi) = F_j(\lambda)\cdot(1 + RV_j(\phi)/c) = \left[F_j(\lambda; p < 1) + F_j(\lambda; p \geq 1)\right]\cdot(1 + RV_j(\phi)/c),$$
where c is the speed of light.
3. *Amalgamation of SEI profiles:* In this third step, these phase-dependent profiles are "combined" at each phase φ into a phase-dependent synthetic Binary-SEI, or BSEI profile $F(\lambda;\varphi)$, taking into account (a) the contribution of each stellar photosphere into UV continuum flux and (b) the published intrinsic photospheric light ratio L_1/L_2 of the member stars in the UV which is 0.6/0.4 (Stickland, Koch, Pachoulakis and Pfeiffer, 1993). The weighing scheme adopted in the calculation of the synthetic BSEI profile $F(\lambda;\varphi)$ assumes disparate winds for the components of the binary that are not seriously deformed from spherically symmetric shapes due to e.g., severe wind collisions.
$$F(\lambda;\phi) \equiv F(\lambda;\phi; p \geq 0) =$$
$$= \left[W_1 \cdot F_1(\lambda; p < 1) + L_1 \cdot F_1(\lambda; p \geq 1)\right]\cdot(1 + RV_1(\phi)/c) +$$
$$\left[W_2 \cdot F_2(\lambda; p < 1) + L_2 \cdot F_2(\lambda; p \geq 1)\right]\cdot(1 + RV_2(\phi)/c)$$

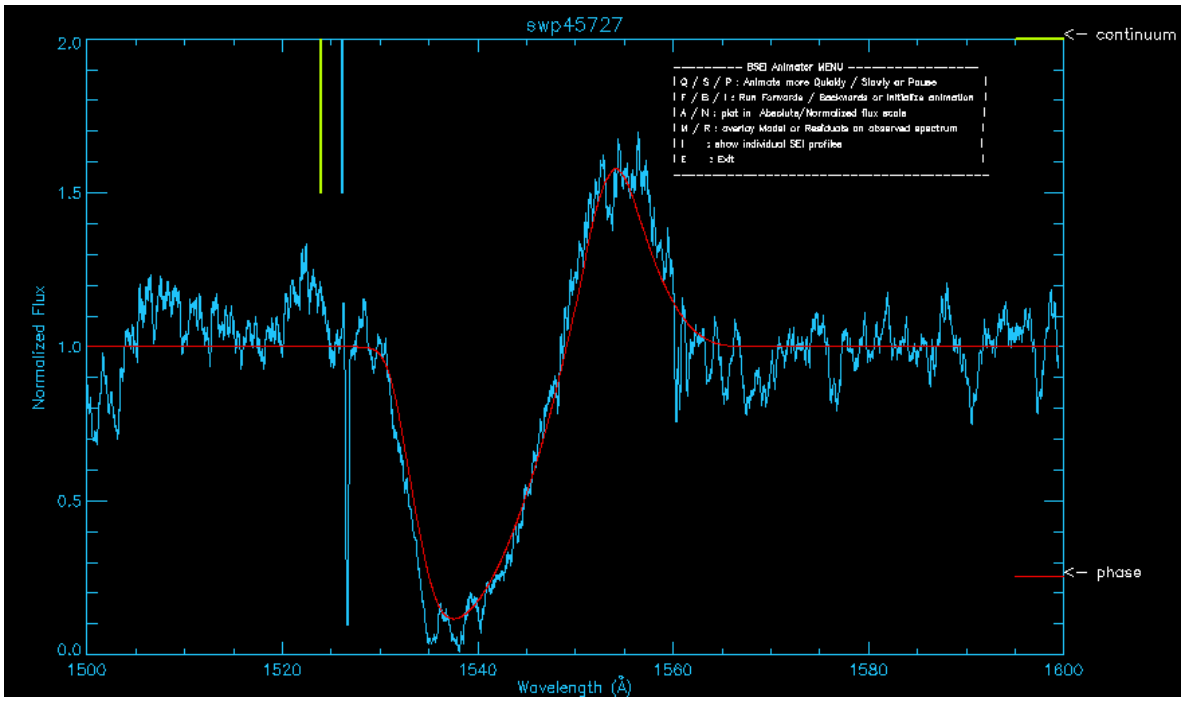

Figure 5. The interface of the Spectrum Analyzer and Animator (SA^2) for wind line profile modeling.

For phases outside photospheric eclipses, $[W_1, W_2] = [L_1, L_2]$, so that the Doppler-shifted SEI profiles (for both $p < 1$ and $p \geq 1$) are weighed according to the intrinsic photospheric light ratio. For phases during photospheric eclipses, $[W_1, W_2] = [LC\text{-}L_1, L_2]$ if the primary star is eclipsed and $[W_1, W_2] = [L_1, LC\text{-}L_2]$ if the secondary star is eclipsed, where LC is the normalized flux measure at that phase derived from the continuum light curves. It is to be noted that a weighing scheme for the $p \geq 1$ contributions cannot be devised because intrinsic "wind" weights are not known and the wind-affected light curve cannot be used as it contains total wind $p \geq 0$ contributions. Accordingly, the weights for the $p \geq 1$ contributions have been kept constant throughout the Keplerian cycle. This procedure is justified because (a) the wind models for these binaries lead to flow times through the line-forming regions of about 2-5% of the Keplerian period and (b) the exposure times of the raw spectral images are only about 30% of the flow time.

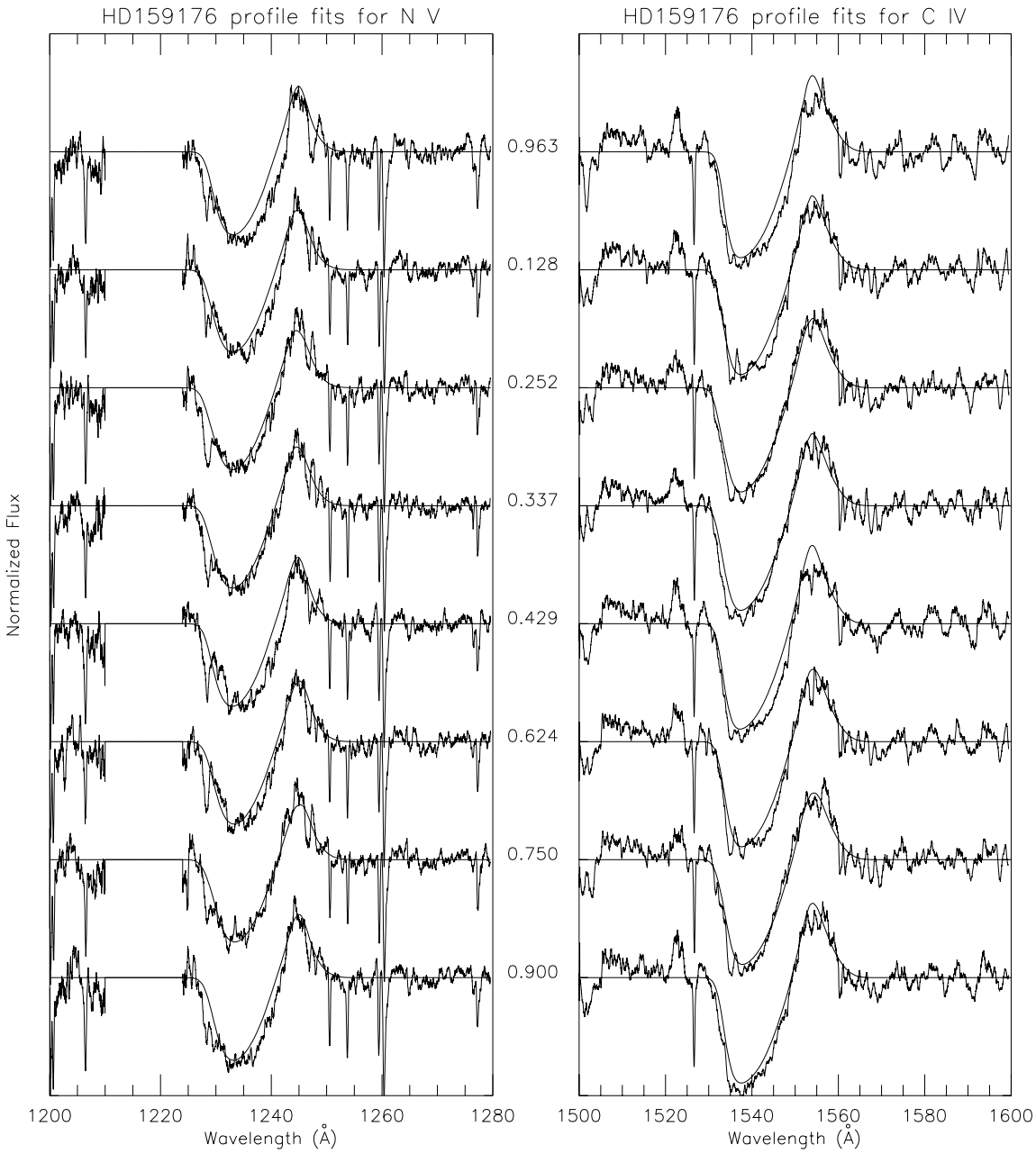

Figure 6. Output of SA^2 showing the BSEI fits to the observed NV and CIV profiles.

Using continuum and wind-affected light curves from Pachoulakis (1996), the observed wind-line profiles are normalized to a continuum flux level of 1.0, so that they can be compared to the synthetic binary wind-line profiles. Finally, truncated spectral intervals centered on the observed wind-line are played back on screen in phase order with their corresponding model line-profiles $F(\varphi)$ superimposed in order to assess the quality of the fit (see Figure 5). The sequence of steps just outlined and beginning with the calculation of new model SEI profiles is iterated until a steady-state composite wind is computed that satisfactorily represents the observed wind-line profiles for each ion.

Figure 6 displays the resultant composite-wind BSEI profiles for the dominant wind lines of HD159176. When perusing this figure, the reader should keep in mind that the phase-locked variabilities of the BSEI model profiles arise solely from the phase-dependent Doppler shifts and the phase-dependent weighting scheme adopted for their creation and represent a steady-state binary wind. The reader may also note that better fits have been attained near quadrature phases than near conjunction phases for both NV and CIV. In fact, as can be seen from Figure 6, these two phases represent the two extremes in quality of fit among all available spectra: the remaining spectra are of intermediate character which varies with phase in a more or less continuous manner between conjunctions and quadratures. The regularity and phase-locked pattern of the fitting quality attests to variability caused by the phase-dependent wind geometry of the binary as observed from Earth.

THE BINARY 3D RENDERER (B3dR)

As discussed in the previous section, the fit quality for the synthetic binary wind-line profiles has been conditioned solely by the requirement that the observed wind profiles be reproduced as faithfully as possible. A way to quantify the quality of the fit is to study the phase-locked patterns of the "model minus observed" - in the sense [BSEI-Observed] - residuals, a process that is automated with the help of the SA[2] as follows:

- First, each (normalized) BSEI profile is multiplied by the same straight-line continuum that was used earlier to normalize the corresponding observed wind-line profile, a process that yields a sequence of model profiles in units of absolute flux.
- Since BSEI does not model line blanketing, each model profile is also multiplied by $1/(1-z)$, where z is the level of line blanketing calculated from the tables of Kurucz (1979) for the appropriate stellar temperature and luminosity in the neighborhood of the wind profile being modeled. As a result, the line-blanketed BSEI model profiles are always brighter than the observed ones.
- Finally, the unmodeled residuals are integrated across the profile and the resulting measures are divided by the profile width to yield average monochromatic flux measures.

Following this recipe, the unmodeled residuals for HD159176 have been computed and modeled (Pfeiffer, Pachoulakis, Koch and Stickland, 1997) using the Binary Wind Interaction (BWI) code developed by R. J. Pfeiffer. BWI uses numerical grids to represent the stellar photospheres, the winds, and an (optional) wind inhomogeneity to partition the residuals into three fundamental categories of wind-interaction effects:

- Eclipses of portions of the remote photosphere, wind, or wind inhomogeneity by the nearer photosphere,
- Attenuations of portions of the remote photosphere, wind, or wind inhomogeneity by the nearer wind and,
- Attenuations of portions of the photospheres and winds of both stars by the wind inhomogeneity.

To aid the visualization of the results, the Binary 3D Renderer (B3dR) has been devised to reconstruct a physically realistic simulation of a binary system which includes the stars, the winds and the wind-interaction effects. Figure 7 shows the organization of the user interface in three vertical panels. The middle (3D graphics) panel renders HD159176 at continuum wavelengths, where the winds and their interaction regions are invisible, so and the observer sees just the two photospheres. The rightmost panel is used to enter stellar, orbital and wind data published in radial velocity and wind analyses which the B3dR uses to compute and render any physical quantity of interest in the graphics panel.

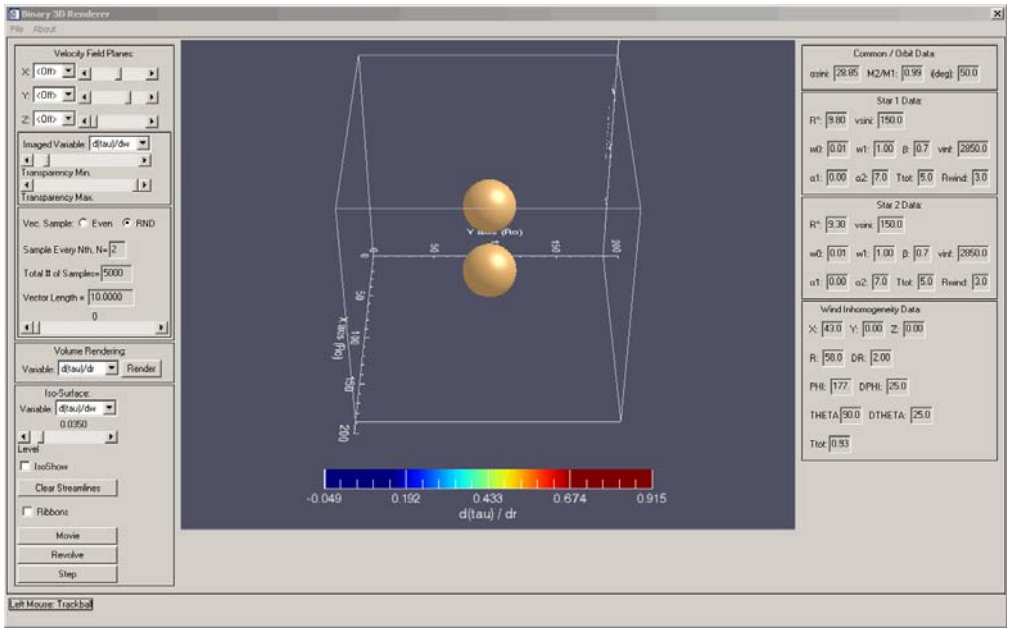

Figure 7. The user interface of B3dR showing the photospheres of HD159176.

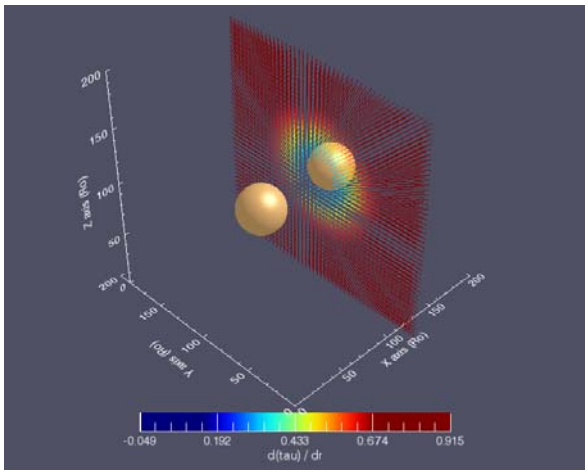

(a) Velocity field plane normal to the line of star centers with regular vector sampling

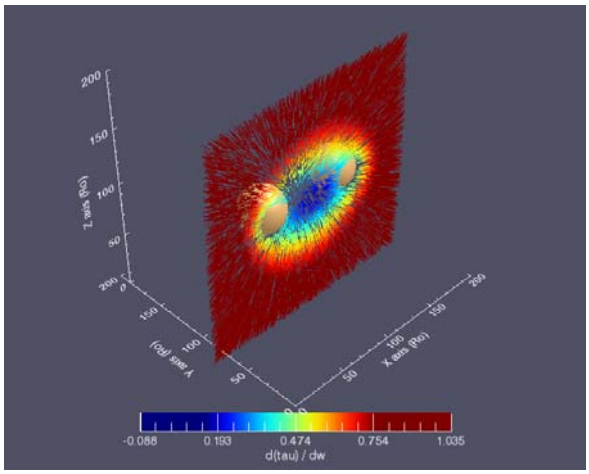

(b) Velocity field plane normal to the Y-axis with random vector sampling

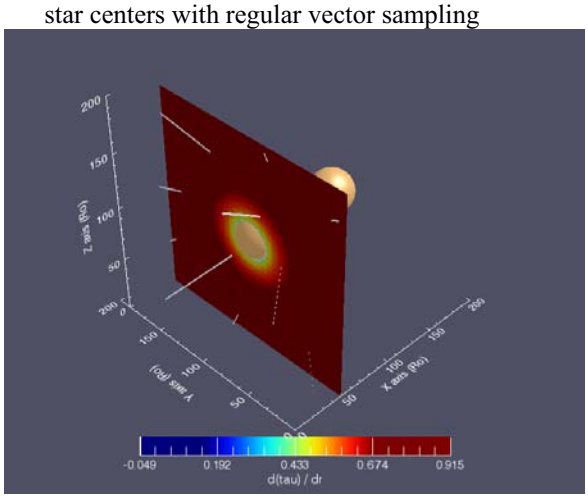

(c) Color-coded velocity field plane with user-placed velocity ribbons

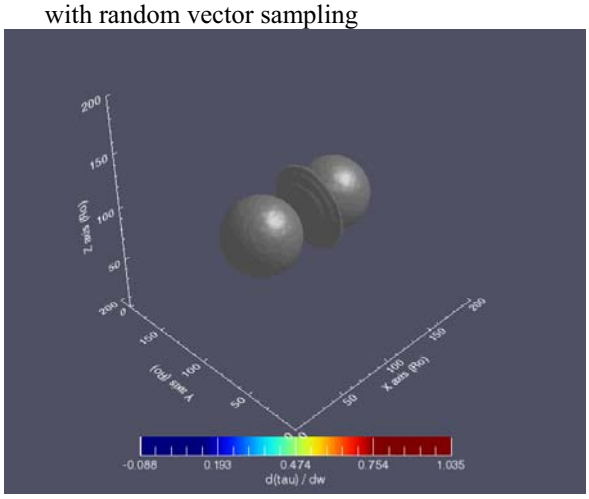

(d) An iso-surface of optical depth

Figure 8. Screen shots of the middle (graphics) panel of B3dR sampling mainstream functionality.

In addition, with the help of the user controls on the leftmost panel, the user may isolate and focus on subsets of data (e.g., slices). Figure 8 shows some of the possibilities: the generation of vector plots for the velocity field at any given location (panels a and b), the production of images from data cross-sections and their annotation with ribbons showing magnitude and direction for the local velocity vector (panel c), as well as iso-surfaces of volume variables such as wind speed, optical depth, etc (panel d).

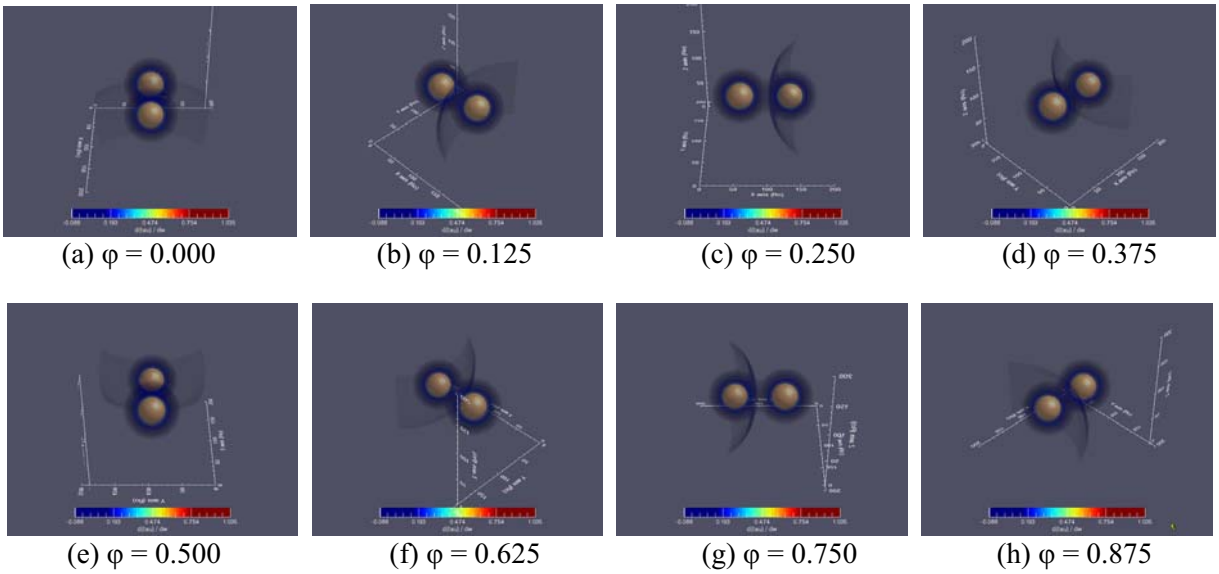

(a) φ = 0.000 (b) φ = 0.125 (c) φ = 0.250 (d) φ = 0.375

(e) φ = 0.500 (f) φ = 0.625 (g) φ = 0.750 (h) φ = 0.875

Figure 9. Schematic representations of HD159176 in B3dR, showing the photospheres, composite wind and wind inhomogeneity at wind-line wavelengths. Panels (a) through (h) show the progress of an orbital cycle in steps of Δφ=0.125, starting from φ=0.0 at the top left. Note: the boxy frame of Figure 8 has been removed and only the three axes appear to avoid screen clutter.

The user may also volume-render physically interesting quantities and produce a simulation of what an observer near the binary system would "see" at wind-line wavelengths. Accordingly, Figure 9 shows a sequence of 3D renderings for HD159176 at CIV wind-line wavelengths and at an inclination of 50^{o} in the course of a single orbital cycle in steps of Δφ=0.125, starting from φ=0.0 in the top left panel. It is exactly these wind-line photons that propagate through these varying geometries in the direction to the observer that are modeled to unlock the structure of the composite wind. In fact, at an inclination $i=0^{o}$ the wind-line profiles of a hot binary would not show any phase-dependent variability at all and the method described in the preceding sections would be quite inapplicable.

DISCUSSION

This article reports on a method used to model, simulate and visualize the 3D structure of astrophysical wind volumes, which operates in a way similar to multi-directional medical tomography in that the spatial structure of an extended target can be reconstructed from a number of spectra obtained by scanning that target from several directions. It is precisely the natural experiments of Keplerian motion and the interactions arising from the presence of a stellar companion that provide the evidence to unlock the structure of each component wind most informatively. Depending on the orientation of the orbit, as the stars trace their Keplerian orbits, one star/wind may be occulted/attenuated by the other star/wind. Accordingly, each photospheric disk – and to a much lesser degree each wind – acts as an analyzing source of light to the front wind. The winds of HD159176 are sufficiently extended and optically thick to deform the wind lines of NV and of CIV into P-Cygni profiles, unmistakable diagnostics of out-flowing material.

The modeling methodology outlined in previous sections uses a custom piece of software, the Spectrum Analyzer and Animator (SA^2) to obtain a physically consistent solution for the binary wind which represents a steady-state composite wind with (possibly) transient features such as wind

inhomogeneities in the circumstellar wind volume. The SA^2 brings together a number of custom-made routines under a common interface and operates in a number of modes to allow the following overall functionalities: extract light curves at continuum and wind-affected bandpasses, normalize the observed spectra and produce synthetic binary wind line (BSEI) profiles which reproduce the observed wind line variabilities. The Binary 3D Renderer (B3dR) is subsequently employed to render the stellar photospheres and the composite binary wind, including the possible wind enhancement(s). Using published orbital data and absolute geometries, this model can be stepped in orbital phase to produce a visualization of what a nearby observer would actually "see" through a pair of spectacles operating at wind-line wavelengths as the stars revolve around their common center of mass.

In addition, the B3dR can be used to visualize the binary winds at any different orbital inclination. For example, at a different orbital inclination the non-eclipsing HD159176 could be made to eclipse and the same modeled binary wind solution would then yield a set of model wind line profiles with amplified phase-locked variability. In fact, among the spectroscopic (Doppler-resolved) OB binary population, those binaries that actually show photospheric eclipses (eclipsing binaries) are the most rewarding, as fundamental stellar parameters such as masses and radii can be accurately recovered from radial velocity and light curve solutions. It is then for such binaries, whose absolute orbital and stellar geometries are well established, that wind structure and interaction parameters can be tightly correlated to fundamental stellar parameters.

Obviously, it is only at the very end of the iterative application of BSEI and BWI that the evidence for wind interaction effects can be collected. Although the present mode of modeling may be unable to recover weak shock fronts, the winds of HD159176 are sufficiently energetic to give rise to an interface shock whose signature is attested by the observed X-Ray surplus from the binary (DeBecker, Rauw, Pittard, Antokhin, Stevens, Gosset and Owocki, 2004; Oskinova, 2005}). In fact, because the stars are not static but revolve in their Keplerian orbits, such a layer does not have to be (and indeed is not) perpendicular to the stellar line of centers.

In summary, the modeling approach discussed in this article provides the grounds for a modeling framework for the understanding of the significantly more extravagant interactions which are of interest in earlier O-type systems, offers a meaningful and consistent method that results in a homogeneous physical parameterization of binary star winds, and provides interactive tools (the SA^2) to automate the analysis of the spectra and visualization tools (the B3dR) which render and explore physically interesting quantities in 3D space. Finally, such physically realistic material can be imported into multimedia authoring tools such as Flash to increase the effectiveness and communication impact of research results. Indeed, undergoing efforts focus on further automating this modeling to be carried out on a web interface.

REFERENCES

DeBecker, M., Rauw, G., Pittard, J. M., Antokhin, I. I., Stevens, I. R., Gosset, E. and Owocki, S. P. (2004). An XMM-Newton observation of the massive binary HD 159176. Astronomy and Astrophysics, 416, 221-233.

Groenewegen, M. A. T. and Lamers, H. J. G. L. M. (1989). The winds of O-stars. I - an analysis of the UV line profiles with the SEI method. Astronomy and Astrophysics Supplement Series, 79(3), 359-383.

Groenewegen, M. A. T., Lamers, H. J. G. L. M. and Pauldrach, A. W. A. (1989). The winds of O-stars. II - The terminal velocities of stellar winds of O-type stars. Astronomy and Astrophysics, 221(1), 78-88.

Hiltner, W. A., Garrison, R. F. and Schild, R. E. (1969). MK Spectral Types for Bright Southern OB Stars. Astrophysical Journal, Vol.157, 313-326.

Kurucz, R. L. (1979). Model atmospheres for G, F, A, B, and O stars. Astrophysical Journal Supplement Series, 40, 1-340.

Lamers, H. J. G. L. M., Cerruti-Sola, M. and Perinoto, M. (1987). The SEI method for accurate and efficient calculations of line profiles in spherically symmetric stellar winds. The Astrophysical Journal, 314, 726-738 (LCP).

Levato, H. (1975). Rotational velocities and spectral types for a sample of binary systems. Astronomy and Astrophysics Supplement Series, 19, 91-99.

Lloyd-Evans, T. (1978). The open cluster NGC 6383. Monthly Notices of the Royal Astronomical Society, 184, 661-676.

Oskinova, L. M. (2005). Evolution of X-ray emission from young massive star clusters. Monthly Notices of the Royal Astronomical Society, 361(2) , 679-694.

Pachoulakis, I. (1996). HD 159176: photospheric and wind-dominated light-curve analyses coupled to wind modeling. Monthly Notices of the Royal Astronomical Society, 1996, 280(1), 153-166.

Perinotto, M., Cerutti-Sola, M. and Lamers, H. J. G. L. M. (1989). Fast winds from the central stars of NGC 6543 and NGC 6826. The Astrophysical Journal, 337, 382-398.

Pfeiffer, J., Pachoulakis, I., Koch, R. H. and Stickland, D. J. (1997). The Winds of Hot Close Binaries. Paper 3: HD159176. The Observatory, 117, 301-309.

Savage, B. D. and Mathis, J. S. (1979). Observed properties of interstellar dust. Annual review of astronomy and astrophysics, 17, 73-111.

Stickland, D. J., Koch, R. H., Pachoulakis, I. and Pfeiffer, R. J. (1993). Spectroscopic binary orbits from ultraviolet radial velocities. Paper 12: HD 159176. The Observatory, 113, 204-209.

Thomas, J. C. (1975). A Photometric Investigation of the Double-Lined O-Star Binary HD 159176. Bulletin of the American Astronomical Society, Vol.7, 533-533.

Thomas, J. C. and Pachoulakis, I. (1994). V and UV Photometry of HD 159176. Information Bulletin on Variable Stars, No. 4115, 1-4.

Ioannis Pachoulakis
Centre for Technological Research of Crete (CTRC)
and Department of Applied Informatics and Multimedia
Technological Educational Institute of Crete
Stavromenos, Heraklion, Crete, GR-71004
Greece
Email: ip@epp.teicrete.gr